Passive modelocking MIR quantum cascade laser incorporating self-induced transparency

A. Outafat, S. Faci, Elodie Richalot, Stephane Protat, Catherine Algani

Passive modelocking MIR quantum cascade laser incorporating self-induced transparency

A. Outafat[1], S. Faci[1*], E. Richalot[2], S. Protat[2] and C. Algani[1]

[1*]ESYCOM, Univ Gustave Eiffel, CNRS, CNAM, 292 Rue Saint-Martin, Paris, 75003, Paris, France.
[2]ESYCOM, Univ Gustave Eiffel, CNRS, 5 Boulevard Descartes, Champs-sur-Marne, 77420, Seine-et-Marne, France.

*Corresponding author(s). E-mail(s): salim.faci@lecnam.net;
Contributing authors: amine.outafat@univ-paris-est.fr;
elodie.richalot-taisne@univ-eiffel.fr ;
stephane.protat@univ-eiffel.fr; catherine.algani@lecnam.net;

Abstract

In this paper, we discuss the passive modelocking of the Quantum Cascade Laser (QCL) incorporating two thin absorbing layers over the gain medium. Based on self-induced transparency (SIT) effect in such structure, it has been demonstrated a potential modelocking by interleaving gain and absorbing layers. We propose here a simplified structure designed by a gain medium surrounded by two thin absorbing layers. To bring out the modelocked stability, we solve the Maxwell-Bloch equations for an open two-level system by the Finite-Difference Time-Domain method (FDTD). As in the case of the interleaved structure, we find similar physical effects on the SIT modelocking in the presence of saturable absorber thin layers. The intensity and the duration of the generated pulses depend strongly on the saturable nonlinearity coefficient and also on the pumping ratio.

Keywords: Quantum Cascade Laser, self-induced transparency, modelocked Laser, Maxwell-Bloch equations, Computational photonics, FDTD

1 Introduction

Mid-infrared (MIR) pulsed laser has many important applications such as high-speed free space communication, time-resolved spectroscopy, coherent control and chemical sensing [1]. One of the most useful sources in the MIR region is the Quantum Cascade Laser (QCL) where photons are generated through intersubband transitions between two energy states located in the conduction band or in the valence band. These transitions are achieved through the engineering of the quantum well structures [2]. The generation of short pulses from QCL in the mid-infrared band has been one of the great challenges since its first demonstration and until today due to the fast gain recovery time of few picoseconds compared to the cavity roundtrip time around 65 ps for a 3 mm cavity length [3], [4]. The QCL modelocking evidence, demonstrating a single pulse generation per roundtrip time, has been achieved experimentally near the threshold pumping current by the active modelocking technique [5], [6]. Passive modelocking of MIR QCL with conventional techniques, such as using saturable absorber or SEmiconductor Saturable Mirror (SESAM) structure [7] are difficult to perform because of the fast gain recovery time. However, thanks to self-induced transparency (SIT) or namely-called coherent phenomena, a passive modelocking of such nonlinear structures of DCL has been proposed in [8], [9]. SIT modelocking is a nonlinear effect demonstrated for the first time by McCall and Hahn [10]. They observed that short pulses above a critical energy, with a duration τ_p shorter than the coherence relaxation time T_2, propagate through an optical medium as if it was transparent. Otherwise, below this critical energy, the pulses vanish. Such pulses are called 2π for which the medium is inverted at the leading edge and the absorbed energy is returned to the pulses at the trailing edge.

Among the various studies of the SIT phenomenon we can mention the work of Kozlov [11] who demonstrate that the technique of coherent passive modelocking may be successfully applied to the different class of media with narrow gain linewidth. Thus, the QCL is suitable for such coherent modelocking technique with specific laser configuration as providing a considerable gain excess over linear interactivity loss. In [12], Talukder *et al.* propose a QCL structure to obtain SIT modelocking by interleaving gain and absorbing layers along the growth axis. In the gain medium, the electrons are injected in the upper-level energy state reaching the population inversion whereas in the absorbing medium, electrons are injected into the lower energy state for a non-inverted population in the resonant state. To reach modelocking, the dipole moment in the absorbing layer should be approximately twice as high as the dipole moment of the active region. In addition, with this structure composed of mixed gain and absorber media, the absorption coefficient could be sufficiently large making the laser not self-start. An auxiliary source is required to initiate the pulse generation as for example by application of an RF signal in a short section the time. Pulse self-starting has been theoretically investigated in a short section laser [13] and in two sections cavity in [14]. The experimental demonstration has been realized with several intractivity designs [15]. In

these experiments, the gain medium consists of Ti:Sapphire and the coherent absorber consists in rubidium cell. Similar structure has been used for THz QCL in which the intensity dependent saturation was implemented with quantum coherent absorber [16]. The authors showed that a fast saturable absorber with a very strong coupling to the optical filed is required accompanied by a careful design of gain medium with a slowly recovering population inversion.

The simulation of such structures was performed by solving Maxwell-Bloch equations with the rotating wave approximation by considering only forward-propagating wave or with simultaneous forward- and backward-propagating waves to consider spatial hole burning [17], [18]. In this paper, we propose a complementary study by simplifying the interleaved structure by a structure composed of multiple gain periods surrounded by two quantum absorbing layers. With this topology, the band-structure engineering complexity is reduced. The light-matter interactions on this structure are analyzed with the two-level approximation of Maxwell-Bloch equations. The simulations are carried out using the Finite-Difference Time-Domain (FDTD) method which achieves time and spatial resolutions of the differential equations based on the Yee's algorithm [19], [20]. This approach does not use any of the standard approximations such as the rotating wave approximation (RWA) or the slowly varying envelope approximation (SVEA). Ziolkowski *et al.* [21] applied the FDTD method to solve the laser dynamics based on Maxwell-Bloch equations for the first time. Then, several works based on this method have been developed to model nonlinear optical effects as for example the active modelocking of terahertz QCL by optical seeding pulse [22] and the dynamics of vertical-cavity surface-emitting lasers [23].

The remainder of this paper is organized in three sections. In the section II, we present the Maxwell-Bloch equations for the proposed structure. In the next one, we discuss about the stability conditions to obtain SIT modelocking and we present the simulation results as function of saturable absorber coefficient values. In the last section, we give a brief conclusion of this work

2 Maxwell-Bloch equations

We have modeled the QCL dynamics with the well-known Maxwell-Bloch equations for an open two-level energy system. These equations describe the interaction between the propagating light and the gain/absorbing medium and are given by [21]:

$$\frac{\partial H_x}{\partial t} = -\frac{1}{\mu_0}\frac{\partial E_z}{\partial y} \tag{1a}$$

$$\frac{\partial E_z}{\partial t} = -\frac{1}{\varepsilon}\frac{\partial H_x}{\partial y} - \frac{\Gamma_g N_g \mu_g}{\varepsilon T_{2,g}}\rho_{a,g} + \frac{\Gamma_g \omega_0 N_g \mu_g}{\varepsilon}\rho_{b,g} - \frac{r_a N_a \mu_a}{\varepsilon T_{2,a}}\rho_{a,a} + \frac{\Gamma_a \omega_0 N_a \mu_a}{\varepsilon}\rho_{b,a} - \left(l_0 - \gamma|E_z|^2\right) E_z \tag{1b}$$

$$\frac{\partial \rho_{a,i}}{\partial t} = -\frac{1}{T_{2,i}}\rho_{a,i} + \omega_0 \rho_{b,i} \tag{1c}$$

$$\frac{\partial \rho_{b,i}}{\partial t} = -\omega_0 \rho_{a,i} - \frac{1}{T_{2,i}}\rho_{b,i} + 2\frac{\mu_i E_z}{\hbar}\Delta_i \tag{1d}$$

$$\frac{\partial \Delta_i}{\partial t} = -2\frac{\mu_i E_z}{\hbar}\rho_{b,i} - \frac{\Delta_i - \Delta_{i0}}{T_{1,i}} + D\frac{\partial^2 \Delta_i}{\partial^2 z} \tag{1e}$$

where E_z is the electric field, H_x is the magnetic field, y is the light propagation axis, the subscript i equals to g for the gain medium and a for the saturable absorber medium, $\rho_{(a,i)}$ and $\rho_{(b,i)}$ represent respectively the dispersive and the absorptive components of the polarization, Δ_i is the fractional difference of the populations for the two energy levels a and b, Δ_{i0} is the equilibrium population inversion away from the modelocked pulse, ω_0 is the atomic transition resonance frequency, μ_i is the electric dipole moment for a two-energy levels atom, N_i is the density of the polarizable atoms, Γ_i is the overlap factor, μ_0 is the free-space permeability, ε is the medium dielectric constant which is the same for the two mediums, l_0 is the linear cavity loss per unit length, γ is the saturable absorber coefficient depending on the active region width [24], $\hbar$ is the Planck constant divided by 2π, D is the dispersion coefficient that models the group velocity dispersion, $T_{(2,i)}$ is the coherence time and $T_{(1,i)}$ is the excited-energy state lifetime in the medium i. The incident electromagnetic field is a uniform plane wave propagating along y-axis and whose electric field is polarized along z-axis.

The fast gain recovery process in QCL is faster than the carrier diffusion leading to spatial hole burning (SHB) effect. This is caused by the standing wave grating which introduces inhomogeneous gain saturation. The dynamic of the QCL is then affected producing a fluctuation of the intensity along the cavity length. Multiple pulse per roundtrip could be exist. The dispersion term D is used here to consider SHB in this simplified structure. For the interleaved structure, the effect of SHB is greatly reduced with the presence of coherent absorption in the laser cavity as discussed in [18]. As for the group velocity dispersion depicted by the coefficient β_2, the intensity and the duration of the pulse can be affected [9]. The modelocking remains stable over critical values of saturable loss and dispersion coefficient. However, these limits depend on the gain and coherent absorption coefficients and a rigorous analysis goes beyond

the scope of the present study. We set the dispersion coefficient β_2 to zero and the complementary analysis will be reported on future work.

In order to obtain SIT modelocking, the gain of the continuous waves must be below threshold. To analyze this issue, we use the derived conditions given in [9] and [12] obtained from Maxwell-Bloch equations with the slowly varying envelope approximation. This is because as described in [19], Maxwell-Bloch equations invoking standard approximations have been effectively used to describe SIT. At threshold, the following relation is obtained [12]:

$$\frac{\Gamma_g k N_g \mu_g^2 \, T_{2,g}}{2\varepsilon_0 n^2 \hbar} \Delta_{g0} + \frac{\Gamma_a k N_a \mu_a^2 \, T_{2,a}}{2\varepsilon_0 n^2 \hbar} \Delta_{a0} - l_0 = 0 \tag{2}$$

which can be written as $g\Delta_{g0} + a\Delta_{a0} - l_0 = 0$, where g and a represent respectively the gain and the quantum coherent absorption per unit length given by:

$$g = \frac{\Gamma_g k N_g \mu_g^2 T_{2,g}}{2\varepsilon_0 n^2 \hbar} \Delta_{g0} \tag{3a}$$

$$a = \frac{\Gamma_a k N_a \mu_a^2 T_{2,a}}{2\varepsilon_0 n^2 \hbar} \Delta_{a0} \tag{3b}$$

with k the wave number, n the refraction index, Δ_{g0} and Δ_{a0} are the equilibrium population inversion at the gain and absorption medium respectively. Expression (2) can be normalized with respect to the internal losses and becomes:

$$\bar{g}\Delta_{g0} + \bar{a}\Delta_{a0} - 1 = 0 \tag{4}$$

with $\bar{g} = \frac{g}{l_0}$ and $\bar{a} = \frac{a}{l_0}$. Simulation of this structure is analyzed following the parameter $\bar{g}$ and with the condition for which the gain is linear below threshold. This means that the left-side of expression (4) stays below zero. Fig. 1 shows the stability limits for an ideal case where the gain layer is fully inverted ($\Delta_{g0} = 1$) and the coherent absorbing layer is fully non-inverted ($\Delta_{a0} = -1$). The first limit condition for continuous waves is written from (4) as $\Delta_g - \Delta_a - 1 = 0$. It is represented by the square points line below which continuous waves grow. The second limit condition, referred by the circle points line, indicates the high limit values for $\bar{a}$ for which the initial pulse is not absorbed. This condition is given by the higher limit of the expression (5) once $T_{2a} = T_{2g}$ [12]. Depending upon the initial conditions Δ_{g0} and Δ_{a0}, these limit curves vary and are associated to different stability conditions.

$$\bar{g} - 1 < \bar{a} < \frac{(3\bar{g} - 2)^2}{12} \tag{5}$$

To obtain stable modelocking, it is necessary to ensure that the ratio $\frac{\varepsilon_a}{\varepsilon_g} > 1$ where the parameters ε_g and ε_a are respectively the nonlinear saturation parameters of the gain medium and the absorbing medium given by expression 6. This condition ensures that the effect of the absorber is greater than the amplification effect of the gain medium.

$$\epsilon_{(a,g)} = \left(\frac{\omega_0}{2\pi\hbar}\right)^2 (T_1 T_2)_(a, g) \tag{6}$$

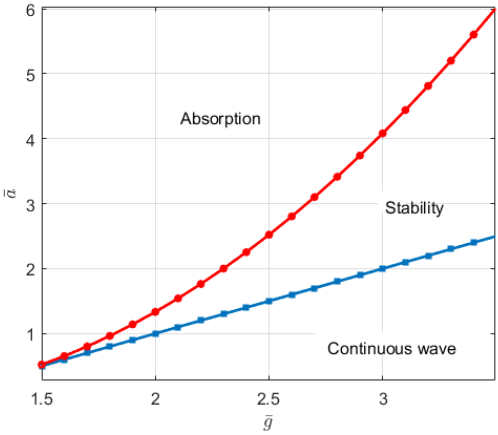

Fig. 1 Stability limit of the normalized coherent absorption as function of the normalized gain

3 Numerical solution for Maxwell-Bloch equations

The one-dimensional FDTD method is used here to solve Maxwell-Bloch equations as a function of time and space [19]. This method is well known for the simulation of many complex cases from RF-structures to light-matter nonlinear interactions [25]. The FDTD method solves the differential equations using the Yee algorithm to calculate the time/spatial derivatives of Maxwell-Bloch equations (1a)-(1e). Time derivatives are replaced by finite differences involving a fixed spatial location at two different times for each variable while the spatial derivatives are replaced by finite differences involving a fixed time at two different spatial locations for each variable. Then, space and time are both discretized with respectively a spatial step Δy and a time step Δt. The resolution of the discretized equations can be performed following different algorithms. For instance, in [21], the predictor-corrector iterative scheme algorithm has been used. The discretized numerical equations for the typical FDTD leap-frog algorithm, in which the electric field E_z and magnetic field H_x propagate along the y-axis, are spatially separated by $\frac{\Delta y}{2}$ and timely separated by $\frac{\Delta t}{2}$, and are given by:

$$H_{x\,m+\frac{1}{2}}^{\,n+\frac{1}{2}} = H_{x\,m+\frac{1}{2}}^{\,n-\frac{1}{2}} - \frac{\Delta t}{\mu_0 \Delta y}\left(E_{z\,m+1}^{\,n} - E_{z\,m}^{\,n}\right) \tag{7a}$$

$$E_{z_m}^{n+1} = E_{z_m}^{n} - \frac{\Delta t}{\varepsilon \Delta y}\left[H_{x_{m+\frac{1}{2}}}^{n+\frac{1}{2}} - H_{x_{m-\frac{1}{2}}}^{n+\frac{1}{2}}\right] - \frac{\Gamma_g N_g \mu_g \Delta t}{\varepsilon T_{2,g}} \rho_{a,g_m}^{n+\frac{1}{2}}$$
$$+ \frac{\Gamma_g N_g \mu_g \omega_0 \Delta t}{\varepsilon} \rho_{b,g_m}^{n+\frac{1}{2}} - \frac{\Gamma_a N_a \mu_a \Delta t}{\varepsilon T_{2,a}} \rho_{a,a_m}^{n+\frac{1}{2}} + \frac{\Gamma_a N_a \mu_a \omega_0 \Delta t}{\varepsilon} \rho_{b,a_m}^{n+\frac{1}{2}} \tag{7b}$$
$$-\Delta t\, l_0 \left(\frac{E_{x_m}^{n+1} + E_{z_m}^{n}}{2}\right) + \Delta t\, \gamma \left(\frac{E_{z_m}^{n+1} + E_{z_m}^{n}}{2}\right)^3$$

$$\rho_{a,i_m}^{n+\frac{1}{2}} = \rho_{a,i_m}^{n-\frac{1}{2}} - \frac{\Delta t}{2T_{2i}}\left[\rho_{a,i}^{n+\frac{1}{2}} + \rho_{a,i_m}^{n-1}\right] + \frac{\Delta t \omega_0}{2}\left[\rho_{b,i_m}^{n+\frac{1}{2}} + \rho_{b,i}^{n-\frac{1}{2}}\right] \tag{7c}$$

$$\rho_{b,i_m}^{n+\frac{1}{2}} = \rho_{b,i_m}^{n-\frac{1}{2}} - \frac{\Delta t\, \omega_0}{2}\left[\rho_{a,i_m}^{n+\frac{1}{2}} + \rho_{a,i_m}^{n-\frac{1}{2}}\right]$$
$$-\frac{\Delta t}{2T_{2,i}}\left[\rho_{b,i_m}^{n+\frac{1}{2}} + \rho_{b,i_m}^{n-\frac{1}{2}}\right] + \frac{\Delta t \mu_i}{\hbar} E_{z_m}^{n}\left[\Delta_{i_m}^{n+\frac{1}{2}} + \Delta_{i_m}^{n-\frac{1}{2}}\right] \tag{7d}$$

$$\Delta_{i_m}^{n+\frac{1}{2}} = \Delta_{i_m}^{n-\frac{1}{2}} - \frac{\Delta t \mu_i}{\hbar} E_{z_m}^{n}\left[\rho_{b,i_m}^{n+\frac{1}{2}} + \rho_{b,i_m}^{n-\frac{1}{2}}\right] + \Delta t \frac{\Delta_{i0}}{T_{1,i}}$$
$$-\frac{\Delta t}{2T_{1,i}}\left[\Delta_{i_m}^{n+\frac{1}{2}} + \Delta_{i_m}^{n-\frac{1}{2}}\right] + \frac{\Delta t}{(\Delta y)^2} D\left[\Delta_{i_{m+1}}^{n-\frac{1}{2}} - 2\Delta_{i_m}^{n-\frac{1}{2}} + \Delta_{i_{m-1}}^{n-\frac{1}{2}}\right] \tag{7e}$$

where the index m corresponds to the spatial step and the index n corresponds to the time step. Compared to the discretized equations of the Ziolkowski *et al.* [21], the coupling method between Maxwell and Bloch equations is different. We use here a simple method that disconnects the Ampere and Bloch equations for which the Bloch equations are discretized at time $(n + 1/2)\Delta t$ and the Maxwell-Ampere equation is discretized at time $n\Delta t$ [26]. This approach yields a more efficient computation that permits a straightforward parallelization and especially for two-dimensional configuration. However, the expression (7b) cannot be directly used to compute next time step of the electric field because of its third order term. In fact, the FDTD algorithm combines future and past values which requires to use specific methods to solve the expression (7b). This kind of equation is well-suited to a predictor-corrector scheme as detail in [21] and [25]. It has been found that the process converges within 3-4 iterations to give a relative difference of 10^{-5} between previous and new values. In this work, we use the Newton-Raphson method to solve the unknown electric field $E_{z_m}^{n+1}$ [27]. This method is an iterative implementation to predict the root of any function and it is based on the function slop to predict the location of the root. The function to solve is derived from expression (7b) in the form:

$$f(x) = \frac{\gamma \Delta t}{8} x^3 + \frac{3\gamma \Delta t}{8} x^2 E_{z_m}^{n} - Ax + B = 0 \tag{8}$$

where $x = {E_z}_m^{n+1}$ is here a variable, ${E_z}_m^n$ is a constant value, A and B are defined as:

$$\begin{aligned} A &= 1 + \frac{\Delta t}{2} l_0 - \frac{3\gamma \Delta t}{8} \left({E_z}_m^n\right)^2 \\ B &= \left(1 - \frac{\Delta t\, l_0}{2}\right) {E_z}_m^n - \frac{\Delta t}{\varepsilon \Delta y} \left[{H_x}_{m+\frac{1}{2}}^{n+\frac{1}{2}} - {H_x}_{m-\frac{1}{2}}^{n+\frac{1}{2}}\right] \\ &- \frac{\Gamma_g N_g \mu_g \Delta t}{\varepsilon T_{2,g}} {\rho_{a,g}}_m^{n+\frac{1}{2}} + \frac{\Gamma_g N_g \mu_g \omega_0 \Delta t}{\varepsilon} {\rho_{b,g}}_m^{n+\frac{1}{2}} \\ &- \frac{\Gamma_a N_a \mu_a \Delta t}{\varepsilon T_{2,a}} {\rho_{a,a}}_m^{n+\frac{1}{2}} + \frac{\Gamma_a N_a \mu_a \omega_0 \Delta t}{\varepsilon} {\rho_{b,a}}_m^{n+\frac{1}{2}} \end{aligned} \tag{9}$$

The root of (8) is determined from the iterative process given by (10) until the convergence is reached. We fixed a target difference of 10^{-8} between the two successive calculated points which is obtained within 3-4 iterations.

$$x_{j+1} = x_j - \frac{f(x_j)}{f'(x_j)} \tag{10}$$

where f' is the derivative function of f, x_{j+1} and x_j are two consecutive values of the electric field.

Once the mathematical formulations are established, the QCL structure of interest in this study is represented in Fig.2. The difference with the structure proposed in [12] concerns the coherent saturable absorbing layers which surround the active region instead of the interleaved gain/absorbing regions. The thickness of absorbing layer is twice that of the gain period to satisfy the dipole moment condition $\mu_a = 2\ \mu_g$. As the thickness of the quantum layers is different, the relaxation times may differ slightly. However, it is reasonable to assume the same value as mentioned in [28] if the gain and absorbing layers are grown from the same material, so then, $T_{1g} = T_{1a}$=T_1 and $T_{2g} = T_{2a} = T_2$. The simulated structure is a 3 mm-length laser cavity ended at its two sides by a 7.5 µm-length air region. An absorbing boundary condition (ABC) is added to the limit of the air regions to emulate the free space operation by implementing a small reflection coefficient at extremities. The initial electric field excitation is applied at the air/QCL interface on the left side, and the propagating electric field can be visualized at any time step and any spatial location along y-axis. It is important to notice that the condition on the dipole moment is not required in the case of two sections laser [14].

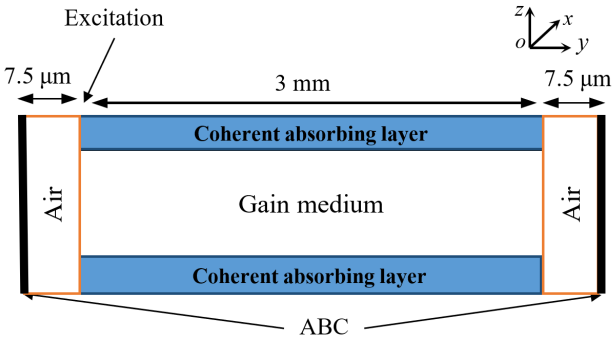

Fig. 2 Laser cavity with coherent absorbing layers. ABC, absorbing boundary layer.

4 Set of physical simulation parameters

The different parameter values of the gain and absorbing regions used in the simulation setup are summarized in Table 1. The same parameters as those given in [29] are selected except for the relaxation time T_1 fixed here at 1ps. As for the saturable coefficient γ, Gordon *et al.* [24] stated the dependence of this parameter on the width of the QCL active region. Thus, we determine here its impact on the SIT modelocking. As mentioned above, the diffusion coefficient β_2 is set to zero. For the FDTD method, we fix the spatial step $\Delta y = 124$ nm and the time step $\Delta t = 41.61$ fs, so that the Courant-Friedrichs-Lewy stability condition $\Delta t \leq \frac{n\Delta y}{c}$ is satisfied.

Table 1 Simulation parameters

Parameters	Symbol	Gain region	Absorbing region
Refractive index	n	3.2	
Gain recovery time	T_l (ps)	1	
Dephasing time	T_2 (fs)	100	
Wavelength	λ (μm)	6.2	
Atom density	$N\left(\mathrm{m}^{-3}\right)$	$6\ 10^{23}$	$1.7\ 10^{22}$
Dipole moment	μ (nm $\times$ e)	2.54	5.08
Diffusion coefficient	$D\left(\frac{cm^2}{s}\right)$	46	
Linear attenuation	$l_0\left(\mathrm{cm}^{-1}\right)$	10	
Overlap factor	Γ	0.96	0.04
Saturable coefficient	$\gamma\left(\frac{m}{V^2}\right)$	$1.9\ 10^{-11}$ ... 0	

The initial pulse is a hyperbolic secant given by the expression (11) where τ_p is the time constant set to 50fs and E_0 the pulse magnitude set to a value giving a π pulse in the gain area and a 2π pulse in the absorbing regions. The calculated value is $E_0 = 5.18\ \frac{MV}{m}$.

$$E(t) = E_0 \,\mathrm{sech}\left(\frac{t}{\tau_p}\right)\sin(\omega t) \tag{11}$$

where ω is the optical carrier frequency taken to be equal to the two-level transition frequency.

5 Simulation results

First, we implemented the developed FDTD method to resolve the Maxwell-Bloch equations. The obtained results in the presence of saturable nonlinearity agree well with those obtained in [9] for the interleaved structure. Thereafter, our analysis starts by setting the normalized gain $\bar{g} = 2.5$ and the quantum absorption coherence at the middle of stability limits represented in Fig. 1, namely $\bar{a} = 2.01$. The saturable absorption coefficient is initially fixed to $1.9\ 10^{-11}\ m/V^2$. The simulation results after 600 roundtrip are represented in Fig. 3. The generated pulse trains in the inset figure show a single pulse per roundtrip with a period of 64 ps which is consistent with the cavity length of the structure. The pulse exhibits a maximum electric field amplitude of 13.4 $\frac{MV}{m}$. The simulation runs 99 ps to allow the output pulses to reach the steady state. From the isolated and normalized pulse, the duration is estimated at 42.6 fs.

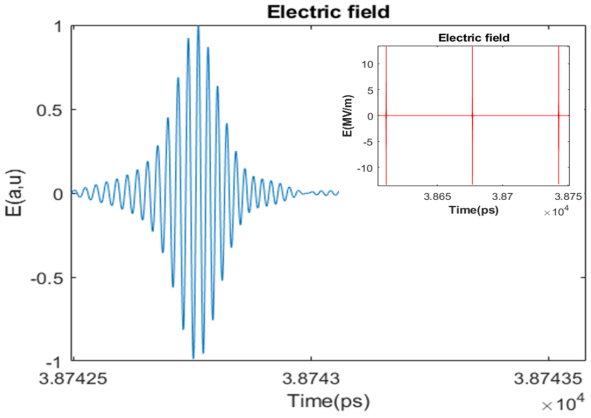

Fig. 3 Normalized electric field pulses for $\bar{g} = 2.5$, $\bar{a} = 2.01$ and $\gamma = 1.9\ 10^{-11}\ \frac{\mathrm{m}}{\mathrm{V}^2}$. The inset figure show the last three generated pulses.

To analyze the effect of the absorber nonlinearity on the generated pulses, we performed several simulations with different values of γ. Two simulation results are given in Fig. 4. When γ is reduced until $10^{-11}\ m/V^2$, the maximum amplitude of the electric field decreases by about 20% and below $10^{-12}\ m/V^2$ the reduction on the peak field amplitude is limited at 38%. This change in γ induces an increase of the pulse width until 54.3fs. Thus, stable modelocked pulses become less intense and broader as γ decreases.

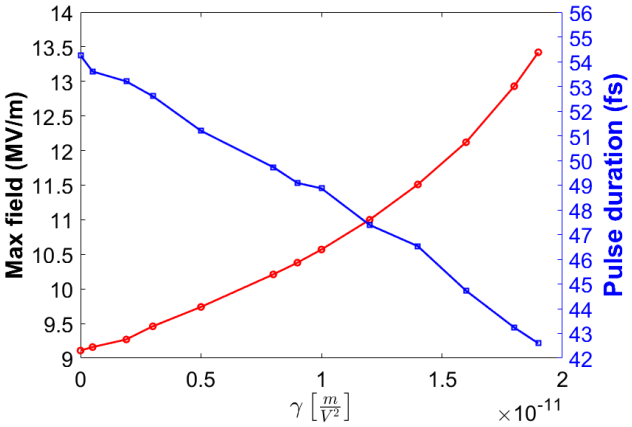

Fig. 4 The maximum optical field and the duration of the stable modelocking pulse versus the saturable nonlinearity coefficient for $\bar{g} = 2.5$ and $\bar{a} = 2.01$.

We now set $\bar{g} = 3.5$ and $\bar{a} = 4.2$ for which the stability is still satisfied. In Fig. 5, we represent the variation of the maximum pulse field and the duration of the generated pulses for different values of γ. We can see the same behavior for the maximum electric field which increases with γ. In comparison to the previous condition, the pulse becomes unstable for nonlinear coefficient $\gamma = 1.9\ 10^{-11}\ m/V^2$. In [30] and [9], this limit for the same $\bar{g}$ and $\bar{a}$ is about $2.8\ 10^{-12}\ m/V^2$. Also, the increase in γ from 0 to $0.9\ 10^{-11}\ m/V^2$ induces a decrease in pulse duration but beyond $0.9\ 10^{-11}\ m/V^2$ the pulse duration increase. The total change is relatively short, only 3 fs over the range of γ values. We can notice a higher maximum intensity and a lower pulse duration once $\bar{g}$ increase.

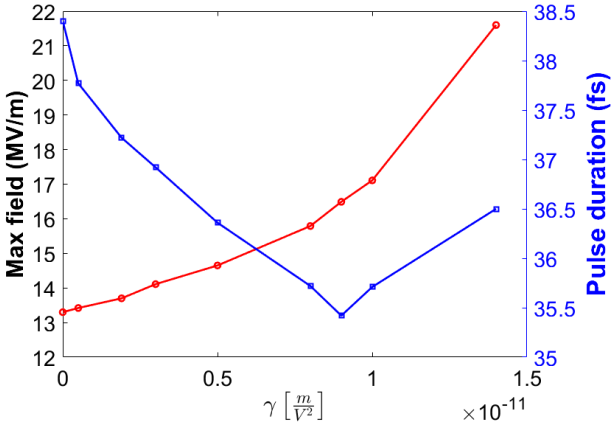

Fig. 5 The maximum optical field and the duration of the stable modelocking pulse versus the saturable nonlinearity coefficient for $\bar{g} = 3.5$ and $\bar{a} = 4.2$

The relaxation time $T_{1,a}$ of the coherent absorber can have an effect on the modelocking stability. To analyze this point, we change the value of $T_{1,a}$ for a fixed gain and coherent absorption coefficients. We use $\bar{g} = 2.5$ and $\bar{a} = 2.01$ inside the stability region, the nonlinear absorption coefficient γ is set to 1.9 10^{-11} m/V^2 and the unchanged dipole moment ν_a. As shown in Fig. 6, the maximum intensity and the pulse duration remain stable for $T_{1,a}$ beyond 1 ps but an important variation is observed when $T_{1,a}$ decreases. When $T_{1a} < 0.25$ ps, the pulse is completely absorbed because the upper stability boundary is slightly lowered. This can be also understanding from expression 6 where ϵ is lower than 1. The modelocking fails when $T_{1,a} > 2$ ps and random pulses appear.

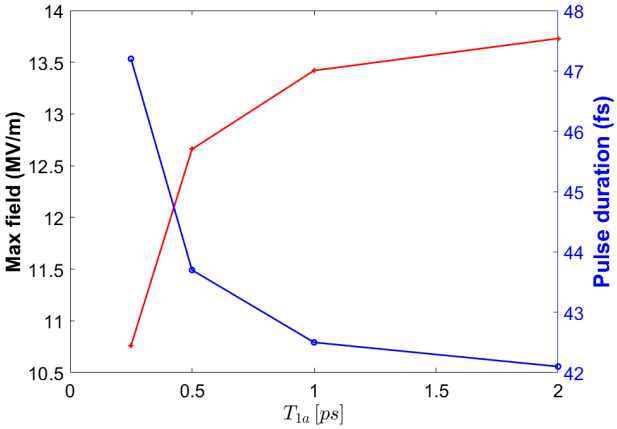

Fig. 6 Effect of $T_{1,a}$ on the generated pulses, $\bar{g} = 2.5$, $\bar{a} = 2$ and $\gamma = 1.9\ 10^{-11}\ \frac{m}{V^2}$.

For parameter values for which the stability condition is not fulfilled as for $\bar{g} = 3.5$ and when $\bar{g}$ is lower than 2.4 corresponding to the limit condition of the stability, the laser dynamics become unstable. Fig.7 shows the establishment of continuous waves instead of stable modelocking. If $\bar{g}$ is set to a value higher than the upper limit, the optical field is totally absorbed. As for example, the simulation with $\bar{g} = 6.1$ has been showed a total absorption of the initial pulse.

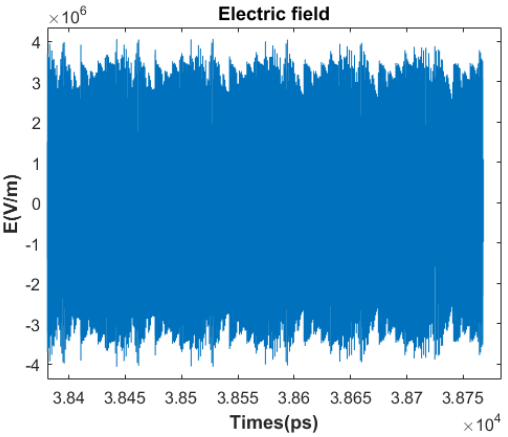

Fig. 7 Output field after 600 round-trip for $\bar{g} = 3.5$, $\bar{a} = 2.4$ and $\gamma = 1.4\ 10^{-11}\ \frac{m}{V^2}$.

6 Conclusion

We have presented in this study a numerical simulation using FDTD method for SIT modelocking of MIR QCL. The FDTD algorithm of Maxwell-Bloch equations have been developed with the weakly coupling method due to its implementation simplicity and parallelization purpose. We showed that with two thin coherent absorbing layers surrounding the multiple gain periods of the QCL cavity, a single pulse per roundtrip can be generated. This configuration is very suitable for modelocking using the SIT effect in the presence of nonlinearity but according to particular stability conditions.

The simulation results for a couple of normalized gain $\bar{g} = 2.5$ and absorption $\bar{a} = 2.01$ have demonstrated a stable modelocking of MIR QCL for different saturable absorber coefficient values. The performances in terms of maximum pulse field and pulse duration are better with a higher value of the saturable absorber coefficient because a higher field amplitude and shorter pulses are obtained. The stability limit for these fixed $\bar{g}$ and $\bar{a}$ values is reached for $\gamma = 1.9\ 10^{-11}\ m/V^2$ for which the amplitude of the electric field is 13.4 $\frac{MV}{m}$ and the pulse duration of 42.6 fs. The change in $\bar{g}$ and $\bar{a}$ modifies the intensity and the duration of the generated pulses where the stability depends on the chosen values. We conclude that the stable SIT modelocking is strongly affected by the presence of saturable absorber nonlinearity compared to the structure with the interleaved gain/absorbing layers.

References

[1] Kosterev, A.A., Tittel, F.K.: Chemical sensors based on quantum cascade lasers. IEEE Journal of Quantum Electronics **38**(6), 582–591 (2002). https://doi.org/10.1109/JQE.2002.1005408

[2] Faist, J., Capasso, F., Sivco, D.L., Sirtori, C., Hutchinson, A.L., Cho, A.Y.: Quantum Cascade Laser. Science (80-.). **264**(5158), 553–556 (1994). https://doi.org/10.1126/science.264.5158.553

[3] Choi, H., Diehl, L., Wu, Z.-K., Giovannini, M., Faist, J., Capasso, F., Norris, T.B.: Gain recovery dynamics and photon-driven transport in quantum cascade lasers. Phys. Rev. Lett. **100**, 167401 (2008). https://doi.org/10.1103/PhysRevLett.100.167401

[4] Choi, H., Norris, T.B., Gresch, T., Giovannini, M., Faist, J., Diehl, L., Capasso, F.: Femtosecond dynamics of resonant tunneling and superlattice relaxation in quantum cascade lasers. Applied Physics Letters **92**(12), 122114 (2008). https://doi.org/10.1063/1.2898518

[5] Gkortsas, V.-M., Wang, C., Kuznetsova, L., Diehl, L., Gordon, A., Jirauschek, C., Belkin, M.A., Belyanin, A., Capasso, F., Kärtner, F.X.: Dynamics of actively mode-locked quantum cascade lasers. Opt. Express **18**(13), 13616–13630 (2010). https://doi.org/10.1364/OE.18.013616

[6] Wang, C.Y., Kuznetsova, L., Gkortsas, V.M., Diehl, L., Kärtner, F.X., Belkin, M.A., Belyanin, A., Li, X., Ham, D., Schneider, H., Grant, P., Song, C.Y., Haffouz, S., Wasilewski, Z.R., Liu, H.C., Capasso, F.: Modelocked pulses from mid-infrared quantum cascade lasers. Opt. Express **17**(15), 12929–12943 (2009). https://doi.org/10.1364/OE.17.012929

[7] Haus, H.A.: Theory of mode locking with a fast saturable absorber. Journal of Applied Physics **46**(7), 3049–3058 (1975). https://doi.org/10.1063/1.321997

[8] Menyuk, C.R., Talukder, M.A.: Self-induced transparency modelocking of quantum cascade lasers. Phys. Rev. Lett. **102**, 023903 (2009). https://doi.org/10.1103/PhysRevLett.102.023903

[9] Talukder, M.A., Menyuk, C.R.: Self-induced transparency modelocking of quantum cascade lasers in the presence of saturable nonlinearity and group velocity dispersion. Opt. Express **18**(6), 5639–5653 (2010). https://doi.org/10.1364/OE.18.005639

[10] McCall, S.L., Hahn, E.L.: Self-induced transparency. Phys. Rev. **183**, 457–485 (1969). https://doi.org/10.1103/PhysRev.183.457

[11] Kozlov, V.V.: Self-induced transparency soliton laser via coherent mode locking. Physical Review A - Atomic, Molecular, and Optical Physics **56**(2), 1607–1612 (1997). https://doi.org/10.1103/PhysRevA.56.1607

[12] Talukder, M.A., Menyuk, C.R.: Analytical and computational study of self-induced transparency mode locking in quantum cascade lasers. Phys.

Rev. A **79**, 063841 (2009). https://doi.org/10.1103/PhysRevA.79.063841

[13] Arkhipov, R., Arkhipov, M., Pakhomov, A., Babushkin, I., Rosanov, N.: Single-cycle-pulse generation in a coherently mode-locked laser with an ultrashort cavity. Phys. Rev. A **105**, 013526 (2022). https://doi.org/10.1103/PhysRevA.105.013526

[14] Arkhipov, R.M., Arkhipov, M.V., Babushkin, I.: Self-starting stable coherent mode-locking in a two-section laser. Optics Communications **361**(c), 73–78 (2016) arXiv:1410.6667. https://doi.org/10.1016/j.optcom.2015.10.030

[15] Arkhipov, M.V., Shimko, A.A., Rosanov, N.N., Babushkin, I., Arkhipov, R.M.: Self-induced-transparency mode locking in a Ti:sapphire laser with an intracavity rubidium cell. Physical Review A **101**(1), 013803 (2020). https://doi.org/10.1103/PhysRevA.101.013803

[16] Tzenov, P., Babushkin, I., Arkhipov, R., Arkhipov, M., Rosanov, N., Morgner, U., Jirauschek, C.: Passive and hybrid mode locking in multi-section terahertz quantum cascade lasers. New Journal of Physics **20**(5) (2018) arXiv:1710.00739. https://doi.org/10.1088/1367-2630/aac12a

[17] Shimu, S.S., Docherty, A., Talukder, M.A., Menyuk, C.R.: Theoretical demonstration of stabilization of active modelocking in quantum cascade lasers with quantum coherent absorption. In: IEEE Photonics Conference 2012, pp. 400–401 (2012). https://doi.org/10.1109/IPCon.2012.6358661

[18] Shimu, S.S., Docherty, A., Talukder, M.A., Menyuk, C.R.: Suppression of spatial hole burning and pulse stabilization for actively modelocked quantum cascade lasers using quantum coherent absorption. Journal of Applied Physics **113**(5), 053106 (2013). https://doi.org/10.1063/1.4790145

[19] Taflove, A., Hagness, S.C., Piket-May, M.: 9 - computational electromagnetics: The finite-difference time-domain method. In: CHEN, W.-K. (ed.) The Electrical Engineering Handbook, pp. 629–670. Academic Press, Burlington (2005). https://doi.org/10.1016/B978-012170960-0/50046-3

[20] Yee, K.: Numerical solution of initial boundary value problems involving maxwell's equations in isotropic media. IEEE Transactions on Antennas and Propagation **14**(3), 302–307 (1966). https://doi.org/10.1109/TAP.1966.1138693

[21] Ziolkowski, R.W., Arnold, J.M., Gogny, D.M.: Ultrafast pulse interactions with two-level atoms. Phys. Rev. A **52**, 3082–3094 (1995). https://doi.org/10.1103/PhysRevA.52.3082

[22] Freeman, J.R., Maysonnave, J., Khanna, S., Linfield, E.H., Davies,

A.G., Dhillon, S.S., Tignon, J.: Laser-seeding dynamics with few-cycle pulses: Maxwell-bloch finite-difference time-domain simulations of terahertz quantum cascade lasers. Phys. Rev. A **87**, 063817 (2013). https://doi.org/10.1103/PhysRevA.87.063817

[23] Bahl, M., Panoiu, N.C., Osgood, R.M.: Modeling ultrashort field dynamics in surface emitting lasers by using finite-difference time-domain method. IEEE Journal of Quantum Electronics **41**(10), 1244–1252 (2005). https://doi.org/10.1109/JQE.2005.855028

[24] Gordon, A., Wang, C.Y., Diehl, L., Kärtner, F.X., Belyanin, A., Bour, D., Corzine, S., Höfler, G., Liu, H.C., Schneider, H., Maier, T., Troccoli, M., Faist, J., Capasso, F.: Multimode regimes in quantum cascade lasers: From coherent instabilities to spatial hole burning. Phys. Rev. A **77**, 053804 (2008). https://doi.org/10.1103/PhysRevA.77.053804

[25] Schlottau, F., Piket-May, M., Wagner, K.: Modeling of femtosecond pulse interaction with inhomogeneously broadened media using an iterative predictor corrector fdtd method. Opt. Express **13**(1), 182–194 (2005). https://doi.org/10.1364/OPEX.13.000182

[26] Bidégaray, B.: Time discretizations for maxwell-bloch equations. Numerical Methods for Partial Differential Equations **19**(3), 284–300 (2003) https://onlinelibrary.wiley.com/doi/pdf/10.1002/num.10046. https://doi.org/10.1002/num.10046

[27] Galántai, A.: The theory of newton's method. Journal of Computational and Applied Mathematics **124**(1), 25–44 (2000). https://doi.org/10.1016/S0377-0427(00)00435-0. Numerical Analysis 2000. Vol. IV: Optimization and Nonlinear Equations

[28] Vukovic, N., Radovanovic, J., Milanovic, V., Boiko, D.L.: Analytical expression for risken-nummedal-graham-haken instability threshold in quantum cascade lasers. Opt. Express **24**(23), 26911–26929 (2016). https://doi.org/10.1364/OE.24.026911

[29] Wójcik, A.K., Malara, P., Blanchard, R., Mansuripur, T.S., Capasso, F., Belyanin, A.: Generation of picosecond pulses and frequency combs in actively mode locked external ring cavity quantum cascade lasers. Applied Physics Letters **103**(23), 231102 (2013). https://doi.org/10.1063/1.4838275

[30] Wang, C.Y., Diehl, L., Gordon, A., Jirauschek, C., Kärtner, F.X., Belyanin, A., Bour, D., Corzine, S., Höfler, G., Troccoli, M., Faist, J., Capasso, F.: Coherent instabilities in a semiconductor laser with fast gain recovery. Phys. Rev. A **75**, 031802 (2007). https://doi.org/10.1103/PhysRevA.75.031802